

# Phonon characteristics and cathodoluminescence of boron nitride nanotubes

Chunyi Zhi, Yoshio Bando, Chengchun Tang, and Dmitri GolbergRongguo Xie and Takashi Sekigushi

Citation: *Appl. Phys. Lett.* **86**, 213110 (2005); doi: 10.1063/1.1938002

View online: <http://dx.doi.org/10.1063/1.1938002>

View Table of Contents: <http://aip.scitation.org/toc/apl/86/21>

Published by the [American Institute of Physics](#)

---

## Articles you may be interested in

[Structure of chemically derived mono- and few-atomic-layer boron nitride sheets](#)

*Appl. Phys. Lett.* **93**, 223103223103 (2008); 10.1063/1.3041639

[Erratum: "Phonon characteristics and cathodoluminescence of boron nitride nanotubes" \[\*Appl. Phys. Lett.\* 86, 213110 \(2005\)\]](#)

*Appl. Phys. Lett.* **87**, 049902049902 (2005); 10.1063/1.2000344

---



# Phonon characteristics and cathodoluminescence of boron nitride nanotubes

Chunyi Zhi,<sup>a)</sup> Yoshio Bando, Chengchun Tang, and Dmitri Golberg

Advanced Materials Laboratory, National Institute for Materials Science (NIMS), Namiki 1-1, Tsukuba, Ibaraki 305-0044, Japan.

Rongguo Xie and Takashi Sekigushi

Nanomaterials Laboratory, National Institute for Materials Science, Namiki 1-1, Tsukuba, Ibaraki 305-004, Japan

(Received 15 March 2005; accepted 26 April 2005; published online 18 May 2005)

Large quantities of highly pure boron nitride nanotubes (BNNTs) are synthesized through a carbon-free method. Nanotube phonon features are investigated by Raman and Fourier-transformed infrared spectroscopies. Both methods indicate highly pure boron nitride phase. Intense ultraviolet light emission is observed when BNNTs are excited by an electron beam, which indicates that the present BNNTs have potential applications in ultraviolet optical devices. © 2005 American Institute of Physics. [DOI: 10.1063/1.1938002]

Boron nitride nanotubes (BNNTs) are structurally stable wide band-gap semiconductors. They have become of significant interest in recent years.<sup>1</sup> The electronic and structural properties of BNNTs have been predicted theoretically, pointing out a wide band gap independent of tube radius, chirality, and the number of tubular shells.<sup>2</sup> This makes BNNTs particularly useful for the nanoelectronic and ultraviolet optical applications.<sup>3,4</sup> However, very few works related to phonon characteristics and luminescence properties of BNNTs have been reported.<sup>4,5</sup> Most reports dealing with BNNTs have been primarily focused on the sole synthesis followed by structural characterization.

Although some methods have been developed to synthesize BNNTs,<sup>6–8</sup> there have been numerous opening questions, e.g., carbon contamination. This markedly hampers the property measurements of BNNTs and their straightforward interpretation. It is noteworthy that recently time-resolved photoluminescence spectroscopy on multiwalled BNNTs, fabricated through a substitution reaction, has been performed by Wu *et al.*<sup>4</sup> The sample contained a mixture of 60–70 vol % BNNTs and 30–40 vol % BN fullerene-like particles. Carbon impurities were also found in the material.

In this letter, highly pure BNNTs were synthesized at a large scale via a carbon-free method,<sup>9–11</sup> Raman and Fourier-transformed infrared (FTIR) spectroscopy were used to investigate the phonon features and phase purity of a sample. Ultraviolet luminescence is observed from BNNTs during cathodoluminescence (CL) experiment, which is analyzed in the framework of BNNT band structure.

The detailed procedure for the synthesis of BNNTs via a carbon-free method is described elsewhere.<sup>11</sup> In brief, a mixture of FeO, MgO, and boron powders was used as the precursor. During heating in an induction furnace, the precursor yields a B<sub>2</sub>O<sub>3</sub> vapor, which is transported to the growth area by an Ar gas and meets with ammonia. After the growth over 2 h, a white flabby BNNT product was collected. The as-grown BNNTs were annealed in N<sub>2</sub> at the temperature of 1700 °C to remove impurities, such as catalyst and MgO phases, etc. Then, the sample was analyzed by scanning

(SEM) and transmission electron microscopies (TEM). SEM investigation displayed that the purity of BNNT can be more than 90 vol %, as shown in Fig. 1. No traces of carbon can be found in the sample, as revealed by electron energy loss spectroscopy (EELS). The BNNTs exhibit a perfect crystalline structure with a diameter of ~50 nm, and a length of up to 10  $\mu$ m.

Raman spectra were collected in a backscattering geometry at room temperature using a Reinshaw 2000 Micro-Raman system employing a 30 mW Ar<sup>+</sup> laser with the wavelength of 514 nm. The typical Raman spectrum of BNNT is similar to that of *h*-BN,<sup>4</sup> as shown in Fig. 2. The dominant peak near 1363.6 cm<sup>-1</sup> can be attributed to the so-called *E*<sub>2g</sub> mode, the well-known counterphase BN vibrational mode within BN sheets. The Raman-active modes of bulk *h*-BN have been investigated, which shows that the high-energy Raman-active *E*<sub>2g</sub> modes are at 1366,<sup>12,13</sup> 1367,<sup>14</sup> and 1370<sup>15</sup> cm<sup>-1</sup>. The *E*<sub>2g</sub> mode of BNNTs is shifted to somewhat lower wave numbers compared with *h*-BN, which may be attributed to the curvature-induced softening.<sup>16</sup> This general trend has also been observed for carbon nanotubes (CNTs).<sup>17</sup> The FWHM of the peak is around 13 cm<sup>-1</sup>. This is

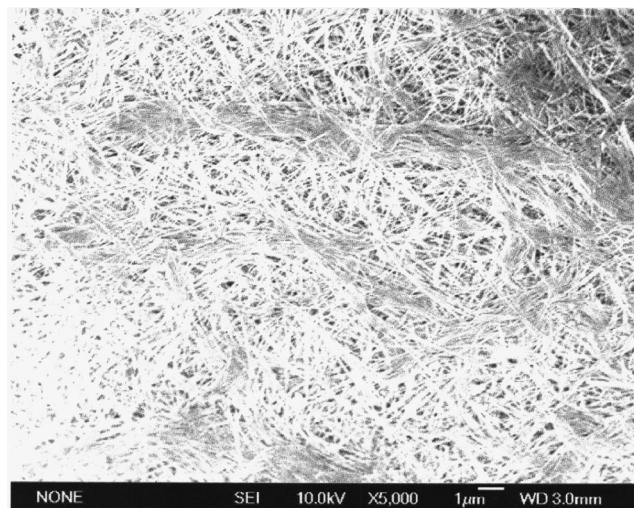


FIG. 1. SEM image of BNNTs.

<sup>a)</sup>Electronic mail: zhi.chunyi@nims.go.jp

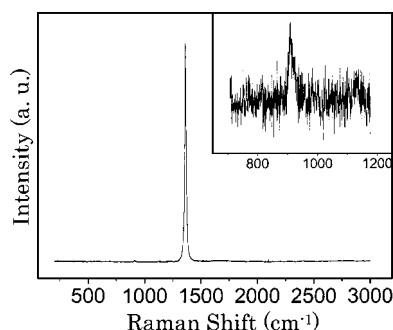


FIG. 2. Raman spectrum of BNNTs. Inset is the enlarged profile of a very weak peak at  $920\text{ cm}^{-1}$ .

wider than in the case of single-crystalline *h*-BN ( $8\text{ cm}^{-1}$ )<sup>18</sup> because of the smaller “crystal size” of BNNTs. However, the regarded value is smaller than in the case of *h*-BN obtained by a chemical vapor deposition method ( $16\text{--}30\text{ cm}^{-1}$ )<sup>19,20</sup> and BNNTs prepared through a substitution reaction ( $17.9\text{ cm}^{-1}$ ).<sup>4</sup> This indicates the better crystallization within the present sample due to a high temperature growth.

As compared to the Raman spectra of boron carbonitride nanotubes (BCNNTs),<sup>21–23</sup> the peak at  $1600\text{ cm}^{-1}$  is lacking. Such a peak would correspond to the  $E_{2g}$  stretching mode of a graphitic-like sheet. In the Raman spectra of graphite, CNTs or BCNNTs, a common feature is the more intense higher-order Raman peaks compared to the first-order peaks. In fact, many materials display the opposite trend. The phenomenon is due to the fact that the higher-order peaks are symmetry allowed in accord with momentum conservation requirement. By contrast, the first order disorder-induced band only appears when there is a breakdown in the in-plane translational symmetry. The second-order Raman peak of BNNTs should be located at more than  $2000\text{ cm}^{-1}$ , however it cannot be identified in Fig. 2. These features reveal the clear difference of Raman characteristics between pure BNNTs and a carbon-containing graphitic structure, although the two structures have similar layered appearance.

The inset of Fig. 2 is an enlarged profile of a very weak peak at  $920\text{ cm}^{-1}$  in the Raman spectrum of BNNTs, which is absent in the Raman spectra of a perfect *h*-BN crystal. The radial breathing modes (RBM) of BNNT is below  $700\text{ cm}^{-1}$  according to the theoretical calculations<sup>24</sup> and usually it is hard to observe RBM in multiwalled nanotubes. It is thought that this peak originates from the lattice distortion, which is similar to the disorder-induced D band at around  $1350\text{ cm}^{-1}$  in Raman spectra of CNTs. The low intensity of this peak is also an indication of high crystallization of the present BNNTs.

More information about the lattice vibrations may be gained through FTIR characterization, which has been performed using a Perkin Elmer FTIR spectrometer with a laser wavelength of  $1024\text{ nm}$ . The typical FTIR spectrum of BNNTs, shown in Fig. 3, is dominated by two peaks at around  $820$  and  $1366\text{ cm}^{-1}$ , which are indexed to represent  $A_{2u}$  (BN vibration perpendicular to the tube axis) and  $E_{1u}$  (BN vibration parallel to the tube axis) modes. As known, BN is a polar material where N is slightly negatively charged, whereas B is slightly positively charged. The long-range character of the Coulomb potential gives rise to a macroscopic electric field  $E$  for longitudinal optical phonons in

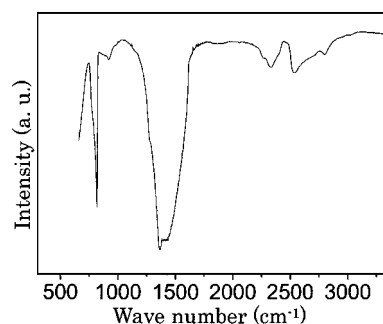


FIG. 3. FTIR spectrum of BNNTs.

the limit  $q \rightarrow 0$ . This results in a splitting (LO-TO splitting) between the longitudinal and transverse optical modes. Although it is predicted that the LO-TO splitting would not take place as long as the diameter of single-walled BNNT bundles is smaller than the wavelength of the laser, it is still believed that splitting exists in the multiwalled BNNTs since there is a long-range dipole-dipole interaction between the walls,<sup>25</sup> that is additionally proved by the present experiment. The  $A_{2u}$  mode is split into  $A_{2u}$  (TO) and  $A_{2u}$  (LO), with a shoulder at  $772\text{ cm}^{-1}$  and a peak at  $820\text{ cm}^{-1}$ , respectively. The  $E_{1u}$  (TO) and  $E_{1u}$  (LO) modes are located at  $1366$  and  $1464\text{ cm}^{-1}$ . Similar to the Raman-active modes, these modes are also softened due to the curvature of a BN sheet comparing with corresponding modes in crystalline *h*-BN.<sup>15</sup>

Although the peak observed at  $920\text{ cm}^{-1}$  is attributed to the high-density two-phonon process in the FTIR studies of *h*-BN,<sup>15</sup> it is thought that this peak has the same origin as the Raman peak at  $920\text{ cm}^{-1}$ . This mode is an IR and Raman active mode and caused by a single phonon process. Origin of the visible shoulder at  $1275\text{ cm}^{-1}$  is still unclear. It is absent in the FTIR spectrum of other BN materials. Furthermore, there are some peaks locating at more than  $2000\text{ cm}^{-1}$ . They may be assigned to multiphonon processes and summing of low frequencies modes.

Intense luminescence is observed while exciting BNNTs with an electron beam. The experiment was performed with a field emission SEM. The spectra excited by different accelerating voltages are shown in Fig. 4, inset is a CL spectrum taken from an individual BNNT. A monotonous increase in the emission intensity was observed as the accelerating voltage increases, while no variation is seen in the position and shape of the dominating peak, located at around  $3.3\text{ eV}$  and tailing off toward a low energy side. A shoulder at  $4.1\text{ eV}$  is more obvious in the spectra excited by high-energy electrons. The ultraviolet light emission was very stable during

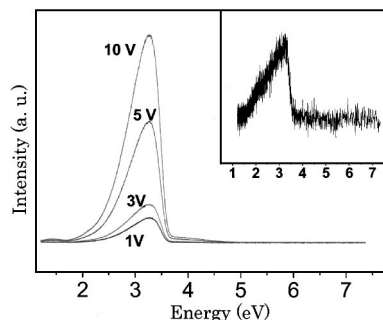


FIG. 4. CL spectra obtained at different accelerating voltages. Inset is CL spectrum obtained from an individual BNNT.

the present experiments. No attenuation was observed after the sample was irradiated for 10 min. This is due to the well-known chemical and thermal stability of BNNTs. The band structure of BNNT has been investigated in both theory and experiments, and the reported band gaps are ranged between 1.7 and 5.4 eV.<sup>2,26–28</sup> Actually, the results may be influenced by the different calculation method and varieties of BNNT structures. For example, in Ref. 27, it has been demonstrated that the band gap of a (7, 0) BNNT is 3.4 eV, whereas a (7, 0) at (15, 0) double-walled BNNT has a band gap of 2.9 eV. It is still difficult to identify the origin of the peak at 3.3 eV. One possibility is that emission is caused by the band-to-band optical transitions across the direct band gap, and the tail locating at a low energy side is caused by B or N vacancy-type defect-trapped states. The other possibility may stand for the fact that both emission at 3.3 eV and the tail are induced by the B and N vacancies, whereas the band-to-band transition is responsible for the shoulder at 4.1 eV. Phonon replica features observed in the photoluminescence of BNNTs<sup>4</sup> do not appear in the CL spectra, which may be caused by a higher temperature during CL measurements.<sup>29</sup>

In summary, highly pure BNNTs have been synthesized at large yield through a carbon-free method. Raman and FTIR techniques have been used to characterize the phonon features of BNNTs. Both methods reveal highly pure well-crystalline boron nitride phase. Intense and stable ultraviolet CL emission has been observed from BNNTs. This makes BNNTs a promising material for ultraviolet optical applications.

The authors thank Dr. Y. Uemura, Dr. M. Mitome, K. Kurashima, and B. D. Liu for their cooperation and kind help.

<sup>1</sup>D. Golberg, Y. Bando, K. Kurashima, and T. Sato, *Scr. Mater.* **44**, 1561 (2001).

<sup>2</sup>X. Blase, A. Rubio, S. G. Louie, and M. L. Cohen, *Europhys. Lett.* **28**, 335 (1994).

- <sup>3</sup>C. Y. Zhi, J. D. Guo, X. D. Bai, and E. G. Wang, *J. Appl. Phys.* **91**, 5325 (2002).
- <sup>4</sup>J. Wu, W. Qian, W. Walukiewicz, J. W. Ager III, W. Shan, E. E. Haller, and A. Zettl, *Nano Lett.* **4**, 647 (2004).
- <sup>5</sup>E. Borowiak-Palen, T. Pichler, G. G. Fuentes, B. Bendjemil, X. Liu, A. Graff, G. Behr, R. J. Kalenczuk, M. Knupfer, and J. Fink, *Chem. Commun. (Cambridge)* **1**, 82 (2003).
- <sup>6</sup>D. Golberg and Y. Bando, *Appl. Phys. Lett.* **79**, 415 (2001).
- <sup>7</sup>D. Golberg, Y. Bando, K. Kurashima, and T. Sato, *Chem. Phys. Lett.* **323**, 185 (2000).
- <sup>8</sup>J. J. Fu, Y. N. Lu, H. Xu, K. F. Huo, X. Z. Wang, L. Li, Z. Hu, and Y. Chen, *Nanotechnology* **15**, 727 (2004).
- <sup>9</sup>C. Tang, Y. Bando, T. Sato, and K. Kurashima, *Chem. Commun. (Cambridge)* **12**, 1290 (2002).
- <sup>10</sup>C. Tang, Y. Bando, and D. Golberg, *J. Solid State Chem.* **177**, 2670 (2004).
- <sup>11</sup>C. Y. Zhi, Y. Bando, C. Tang, and D. Golberg (unpublished).
- <sup>12</sup>T. Kuzuba, K. Era, T. Ishii, and T. Sato, *Solid State Commun.* **6**, 523 (1968).
- <sup>13</sup>R. J. Nemanich, S. A. Solin, and R. M. Martin, *Phys. Rev. B* **23**, 6348 (1981).
- <sup>14</sup>D. M. Hoffman, G. L. Doll, and P. C. Eklund, *Phys. Rev. B* **30**, 6051 (1984).
- <sup>15</sup>R. Geick, C. H. Perry, and G. Rupprecht, *Phys. Rev.* **146**, 543 (1966).
- <sup>16</sup>L. Wirtz, A. Rubio, R. A. de la Concha, and A. Loiseau, *Phys. Rev. B* **68**, 045425 (2003).
- <sup>17</sup>O. Dubay and G. Kresse, *Phys. Rev. B* **67**, 035401 (2003).
- <sup>18</sup>T. Kuzuba, K. Era, T. Ishii, and T. Sato, *Solid State Commun.* **25**, 863 (1978).
- <sup>19</sup>D. M. Hoffman, G. L. Doll, and P. C. Eklund, *Phys. Rev. B* **30**, 6051 (1984).
- <sup>20</sup>R. Geick, C. H. Perry, and G. Rupprecht, *Phys. Rev.* **146**, 543 (1966).
- <sup>21</sup>C. Y. Zhi, X. D. Bai, and E. G. Wang, *Appl. Phys. Lett.* **80**, 3590 (2002).
- <sup>22</sup>C. Y. Zhi, X. D. Bai, and E. G. Wang, *Appl. Phys. Lett.* **84**, 1549 (2004).
- <sup>23</sup>M. J. Matthews, M. A. Pimenta, G. Dresselhaus, M. S. Dresselhaus, and M. Endo, *Phys. Rev. B* **59**, R6585 (1999).
- <sup>24</sup>D. Sánchez-Portal and E. Hernández, *Phys. Rev. B* **66**, 235415 (2002).
- <sup>25</sup>L. Wirtz, A. Rubio, R. A. de la Concha, and A. Loiseau, *Phys. Rev. B* **68**, 045425 (2003).
- <sup>26</sup>Y. Kim, K. J. Chang, and S. Louie, *Phys. Rev. B* **63**, 205408 (2001).
- <sup>27</sup>S. Okada, S. Saito, and A. Oshiyama, *Phys. Rev. B* **65**, 165410 (2002).
- <sup>28</sup>G. G. Fuentes, E. Borowiak-Palen, T. Pichler, X. Liu, A. Graff, G. Behr, R. J. Kalenczuk, M. Knupfer, and J. Fink, *Phys. Rev. B* **67**, 035429 (2003).
- <sup>29</sup>W. J. Zhang, H. Kanda, and S. Matsumoto, *Appl. Phys. Lett.* **81**, 3356 (2002).